**Zeitschrift:** Helvetica Physica Acta
**Band:** 58 (1985)
**Heft:** 2-3

**Artikel:** Dendritic single crystals : microstructure and deformation behaviour
**Autor:** Blank, E. / Kurz, W. / Rappaz, M.
**DOI:** https://doi.org/10.5169/seals-115614

Helvetica Physica Acta, Vol. **58** (1985) 469–483

0018–0238/85/020469–15$1.50 + 0.20/0


# Dendritic single crystals: Microstructure and deformation behaviour

By E. Blank, W. Kurz and M. Rappaz

Ecole Polytechnique Fédérale de Lausanne, Département des Matériaux, 1007 Lausanne

(24. IX. 1984)

In honor of Emanuel Mooser's 60th birthday

*Abstract.* In the solidification of metals, liquid–solid phase transformations commonly occur by the growth of dendrites. Dendritic single-crystals produced by directional solidification can contain hundreds of dendrites which, in the as-solidified state, are outlined by segregation products. This paper reviews the present understanding of dendrite growth and describes the crystallographic perfection of dendritic single-crystals. Furthermore, it is shown how the mechanical properties of these crystals are influenced by the distribution of segregation products. This distribution is closely related to the solidification process.

## 1. Introduction

Technology has been strongly influenced by the arrival of mass produced single crystals. This is common statement in the field of physics and electronics where pure, highly homogeneous crystals are used for electronic or optical devices. In mechanical engineering however, one had to wait for the development of a different kind of single crystal in order to overcome the extremely low yield strength of pure metals. These new materials are alloyed, inhomogeneous single crystals consisting of a dendritic microstructure with large amounts of segregation products and precipitates which strengthen the material (Fig. 1). They also contain many growth defects, particularly subgrain boundaries between the dendrites.

Dendritic single crystals are presently used as high temperature materials in aircraft engines. It was in the early sixties that the directional solidification techniques for growing monocrystalline turbine blades were developed by Pratt & Whitney (Fig. 2). The reason for this development was the much improved creep and thermal cycling behaviour of the monocrystalline superalloys as compared to the polycrystalline ones: by elimination of the high angle grain boundaries the weakest areas of the material had been removed [1].

Monocrystalline dendritic turbine blades are made from superalloys containing up to 12 elements within well defined narrow compositional ranges. Macroscopically, these elements should be equally distributed to achieve uniform properties. On a microstructural scale, however, inhomogeneities acting as obstacles for the movement of dislocations are necessary to obtain mechanical strength. Den-

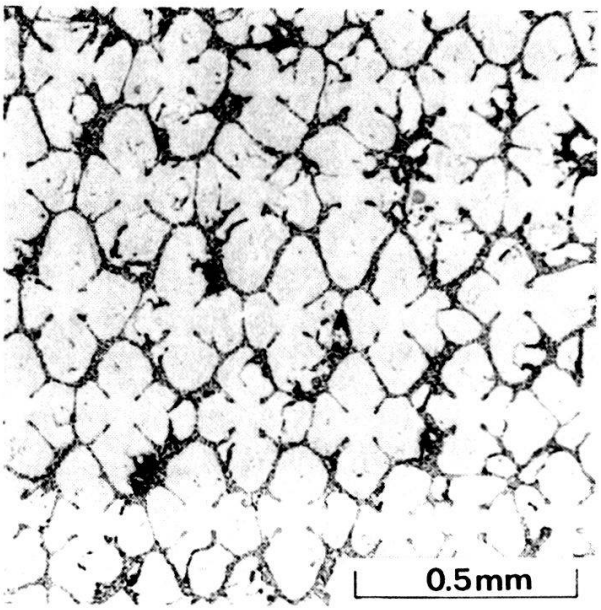


Figure 1
Transverse section of a Ni-22.2 at % Cr-3.6 at % C single crystal.

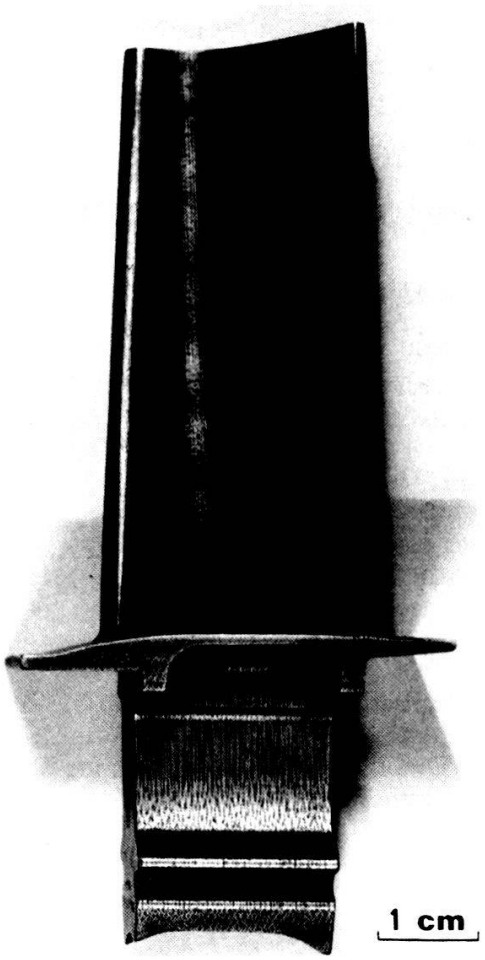


Figure 2
Monocrystalline turbine blade for aircraft application. Such turbine blades are made from Ni-base superalloys using a modified Bridgeman crystal growth technique.

dritic solidification is a prerequisite to avoid macrosegregation.[1]) Solute rejection at the solid–liquid interface however leads to microscopic inhomogeneities in the size range of the dendrite arm spacing $\lambda_2$, typically varying from 10 to 100 $\mu$m (microsegregation). For optimum mechanical properties, obstacle spacings of about 10 to 100 nm are required. High-strength cast products therefore must undergo a so called solutionizing heat treatment[2]) prior to precipitation of fine spaced particles from the solid state. For commercial reasons, solutionizing which is a slow process is always incomplete, even in the case of the extremely expensive turbine blade materials. Thus, the microstructures of alloyed castings represent an agglomeration of solid state and liquid state phase transformation products which both influence mechanical properties.

Dendritic single crystals are not only of interest for gas turbines. They also form the basis of any casting as each grain of a polycrystalline alloy is a single crystal.

---

[1]) In casting technology, macrosegregation may be a severe problem which is related to convectional flow rather than to diffusional solute segregation.

[2]) Solutionizing means dissolution of microstructural inhomogeneities by high temperature diffusion in the solid state. If the dissolution is complete, solutionizing and homogenization are equivalent terms.

Precise knowledge of the mechanical behaviour of individual dendritic grains is necessary if the behaviour of cast alloys is to be understood and if better alloys for the future are to be designed. Within the framework of the Swiss National Program on 'Materials and Materials Resources', the latter subject has been tackled for the first time for dendritic two-phase single crystals, in a way as Schmid did it in the early thirties for pure metal single crystals [2]. The main difficulty for understanding dendritic single crystals is the great complexity of the distribution of alloying elements and precipitates which are related to the morphology and size of the dendrites forming the solidification front of such materials. In this paper a combined approach of microstructure formation and deformation behaviour will be presented in order to demonstrate how control of the solidification conditions influences mechanical properties.

## 2. Microstructure

Figure 3 shows a dendritic crystal exhibiting a heavily branched structure. The dendrite arms are oriented along simple crystallographic directions which, in the case of cubic metals, are the ⟨100⟩ axes. In recent years, the theory of dendrite tip growth has made good progress as a result of application of the perturbation theory to the transport solutions of a growing needle crystal of paraboloidal shape [3]. But the theoretical description of dendrite trunk and arm spacings is still in its

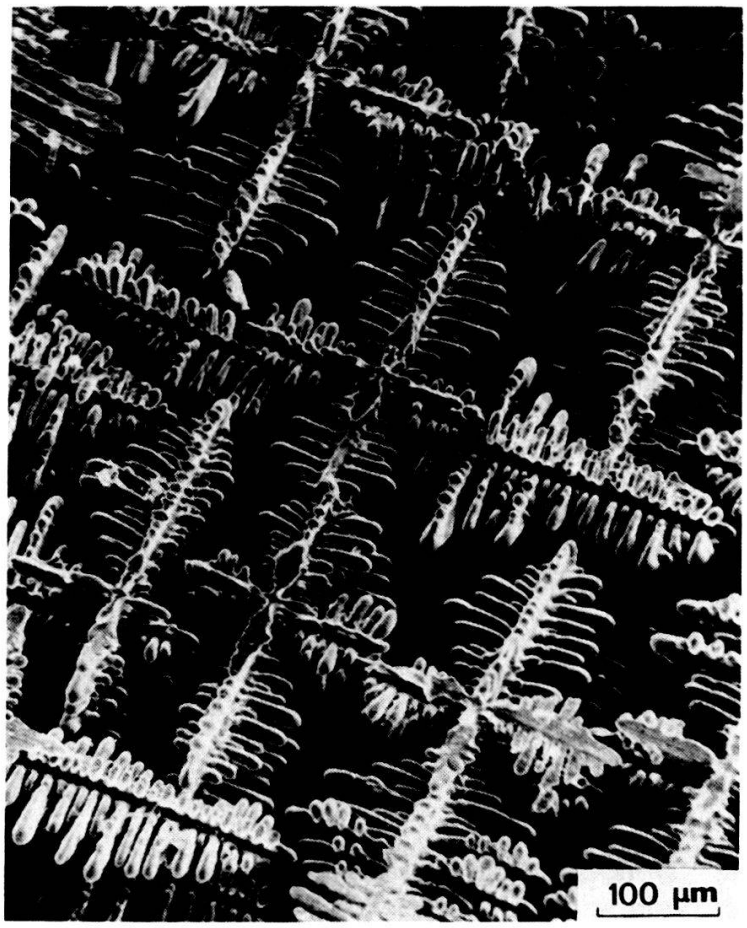


Figure 3
Co-dendrite during growth after eliminating the liquid phase.

infancy. Nevertheless, it is important to be able to predict at least qualitatively the microstructural parameters in order to control mechanical properties.

### 2.1. *Formation of dendrites*

In most practical cases, the planar solidification front of an alloy is unstable as a result of the rejection of solute ahead of the interface. Using a stability criterion, one finds that the typical wavelength of the instability is given by [4]:

$$\lambda_i = 2\pi\sqrt{\frac{\Gamma}{mG_c - G}} \tag{1}$$

where $\Gamma$ is the Gibbs–Thomson coefficient (i.e. the ratio of the solid–liquid interface energy over the entropy of fusion), $m$ the slope of the liquidus, $G_c$ and $G$ the solute and thermal gradients at the solid–liquid interface.

Once the interface has become unstable and is no longer planar, the modelling of the growth front becomes difficult since the rejection of solute is strongly dictated by the complicated dendrite morphology. However, the tip of $\alpha$ dendrite grows at the limit of stability which means that its radius of curvature $R$ is close to $\lambda_i$. On the other hand, the assumption $G \ll mG_c$ applies reasonably well for most dendritic growth conditions. Therefore:

$$R = 2\pi\sqrt{\frac{\Gamma}{mG_c}} \tag{2}$$

The solute gradient at the tip may be calculated from a mass balance which states that, under steady-state conditions, the rejection of solute $c^*(1-k)\cdot v$ from the solid is equal to the solute flux $-DG_c$ diffusing into the liquid. $k$ is the distribution coefficient (i.e. the ratio of the solute concentration in the solid, $c^*k$, over that in the liquid, $c^*$ at the tip), $v$ the growth rate and $D$ the diffusion coefficient. Replacing $G_c$ in equation (2), one obtains:

$$R = 2\pi\sqrt{\frac{\Gamma \cdot D}{vk\ \Delta T_0}} \tag{3}$$

with $\Delta T_0$, the solid–liquid temperature interval, being equal to $m(C_0/k)(1-k)$.[3])

The tip radius which characterizes the solidification kinetics can be correlated with the microstructural parameters such as the diameter, $d$, of the dendrite trunks, the dendrite trunk spacing, $\lambda_1$, and the dendrite arm spacing, $\lambda_2$. The trunk diameter, $\alpha$, is situated in the range of 5–10 tip radii. The primary trunk spacing $\lambda_1$ can be calculated from $R$, assuming that the overall dendrite morphology, including the secondary branches, is approximated by an ellipsoid of revolution. One finds [4]:

$$\lambda_1 = 4.3\left(\frac{D\Gamma\,\Delta T_0}{k}\right)^{1/4} v^{-1/4} G^{-1/2} \tag{4}$$

Therefore primary trunk spacing depends only on the growth conditions. The secondary spacing $\lambda_2$ depends also on solidification time. The initial spacing close

---

[3]) The approximation $c^* \approx c_0$ has been made which means that the tip undercooling is small compared to $\Delta T_0$.

to the tip, $\lambda_2'$, is simply related to $R$ by $\lambda_2' \simeq 2R$. However, this spacing coarsens inside the mushy zone[4]) due to the curvature differences and due to diffusional transport between neighbouring arms being in contact with the melt. A simple analysis of this ripening phenomena (written here, in a slightly modified way) gives a $t^{1/3}$ law [5]:

$$\lambda_2^3 - (\lambda_2')^3 = (5.5)^3 \cdot M \cdot t_f \tag{5}$$

where $\lambda_2$ is the final spacing for a local solidification time, $t_f$, and

$$M = \frac{\Gamma D \ln (C_e^m/C_0)}{m(1-k)(C_e^m - C_0)}$$

$C_e^m$ which is the composition of the last solidifying liquid, is often equal to the eutectic composition.

The increase in solid fraction inside the mushy zone leads to non-equilibrium segregation resulting in the precipitation of second phases, often in the form of interdendritic eutectic. The approximate volume fraction of that precipitation, *fe*, can be obtained from a mass–balance equation and taking into account the back-diffusion in the solid. One gets:

$$fe = 1 - \left(\frac{1}{1-2\Omega K}\right)\left[1 - \left(\frac{C_e}{C_0}\right)^{(1-2\Omega k)/(k-1)}\right] \tag{6}$$

where $\Omega(\alpha)$ is a function of a dimensionless back-diffusion parameter $\alpha = D_s t_f / L^2$, with $D_s$ being the diffusion coefficient in the solid and $L$ a typical dimension (e.g. $\lambda_2$) [4].

Figure 4 shows the application of some of the relationships discussed for a model alloy Ni–Cr–C. Further comparison of the microstructural models with experiments on superalloys can be found in [6]. They show that a reasonable prediction of the scale of the microstructure can be made by present theory.

## 2.2. *Orientation distribution of dendrites*

Dendritic single crystals contain three major kinds of imperfections. First, the composition of cast alloys is inhomogeneous. Second, particles of intermediate phases may precipitate within the dendrites and on interdendritic boundaries. Third, the rapid and not always symmetric growth of individual dendrites induces strains during the solidification process which give rise to crystallographic misorientations between adjacent dendrites.

X-ray diffraction is the most sensitive method for the determination of crystallographic lattice orientations and lattice spacings' variations. Berg–Barrett topography, with a spatial resolution of about 5 microns, permits to obtain dark-field images of zones typically of 1 cm$^2$. Semiquantitative correlations can be established between the orientations of numerous dendrites. Furthermore, subgrain contrasts within individual dendrites can be visualized. As an example, the topograph of a (001) cross section of a dendritic single crystal turbine blade is shown in Fig. 5. The area is about 10 mm by 5 mm. This topograph was recorded using the asymmetric. Ni-fcc (113) reflection with Cu-K$\alpha$ radiation. Diffracting

---

4) The term 'mushy zone' denotes the two-phase region in a solidifying alloy with coexistance of the liquid and the solid phases.

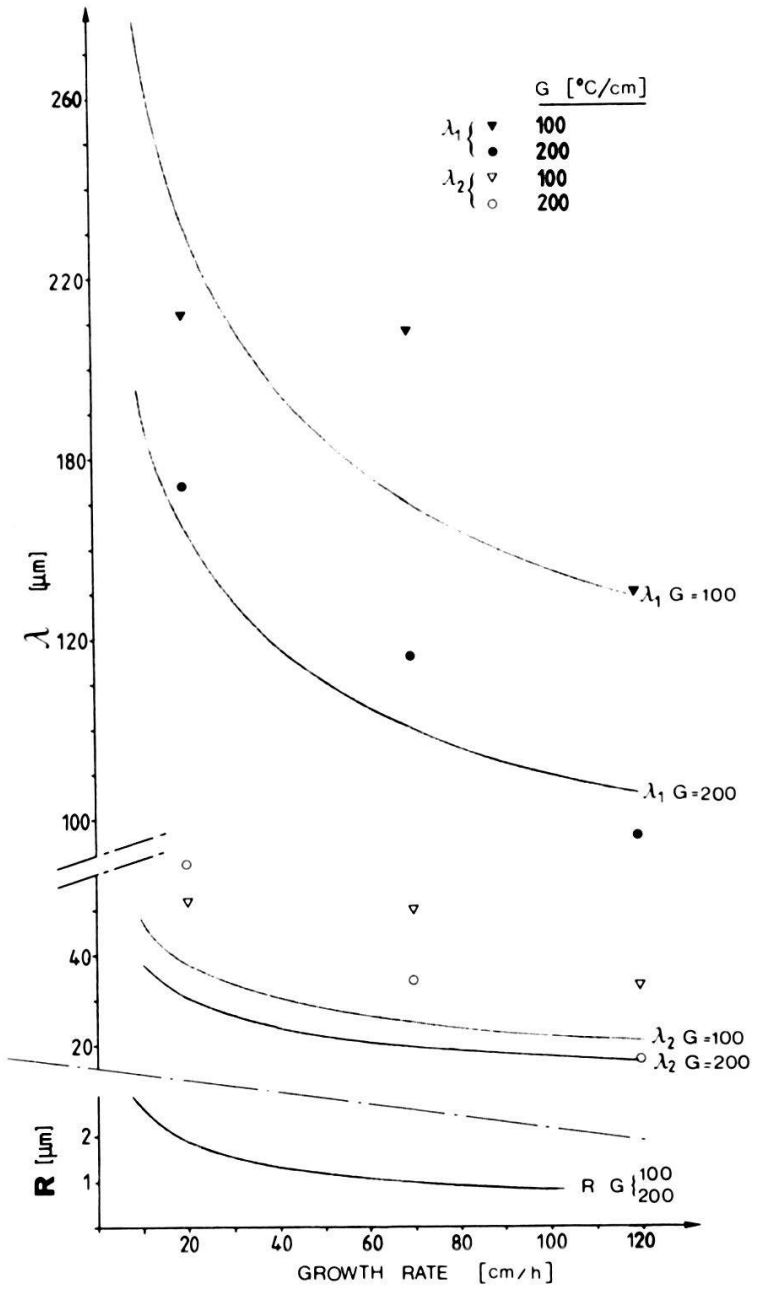


Figure 4
Comparison between measured and calculated values of dendrite spacings $\lambda_1$, $\lambda_2$ and tip radius $R$ as a function of the growth rate $v$.

dendrites appear in dark. Depending on the angular setting of the specimen, different sets of dendrites are oriented for diffraction as can be seen by comparison of Figs. 5a and b. If the specimen and the film are continuously rocked by $\pm 0.5°$ during exposure (*c*), almost all dendrites diffract leaving only displacement contrasts to appear on the topograph. Such observations yield straightforward information about the crystallographic orientation distribution of dendrites belonging to the same crystal.

Topographic informations can be complemented by quantitative diffractometric measurements. Using a recently developed technique for X-ray topography and X-ray microbeam diffraction ($\geqslant 50\ \mu$m beam diameter), X-ray diffraction has been applied to analyse the crystallographic perfection of dendritic

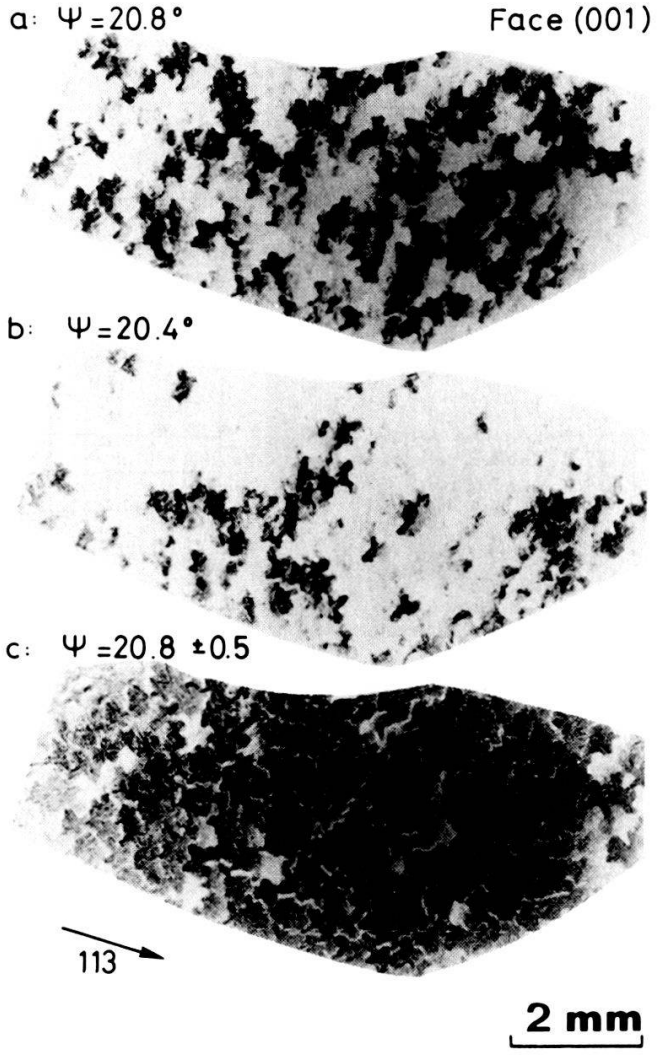


Figure 5
X-ray topographs taken from a (001) transverse section of the turbine blade shown in Fig. 2, (113) reflection. Depending on the orientation of the turbine blade with respect to the X-ray beam, different dendrites are diffracting in a and b as a result of small crystallographic misorientations between individual dendrites. In c almost all dendrites are diffracting (see text).

microstructures [7]. By this technique a spatial resolution of the same order as the beam diameter can be achieved ($\sim 50\,\mu$m) in addition to a lattice spacings' resolution of $\Delta d/d = 10^{-4}$ and a resolution for lattice misorientations of $5 \cdot 10^{-3}$ degrees. In Fig. 6, the (001) orientations of the individual dendrites of a model alloy Ni–Cr–C alloy have been accurately determined. By translation of the specimen with respect to the X-ray microbeam, the orientation of the dendrite trunks numbered 1 to 15 (Fig. 6a) were measured individually. The results were reported in the extended stereographic projection of Fig. 6b where the angle $\theta = 0$ corresponds to the normal of the specimen surface shown in Fig. 6a. $\theta = 0$ represents also the direction of solidification. The choice of dendrites 1 to 15 was based on topographical observations indicating that the microstructure of Fig. 6a was tricrystalline. The grain boundary outlined by a heavily drawn contour line was revealed by X-ray topography. It is interesting to note that the orientations of dendrites 12, 5, 13, 14 and 15 (Fig. 6b) which all touch the grain boundary, are situated on a path extending from the bottom right corner to the upper left corner

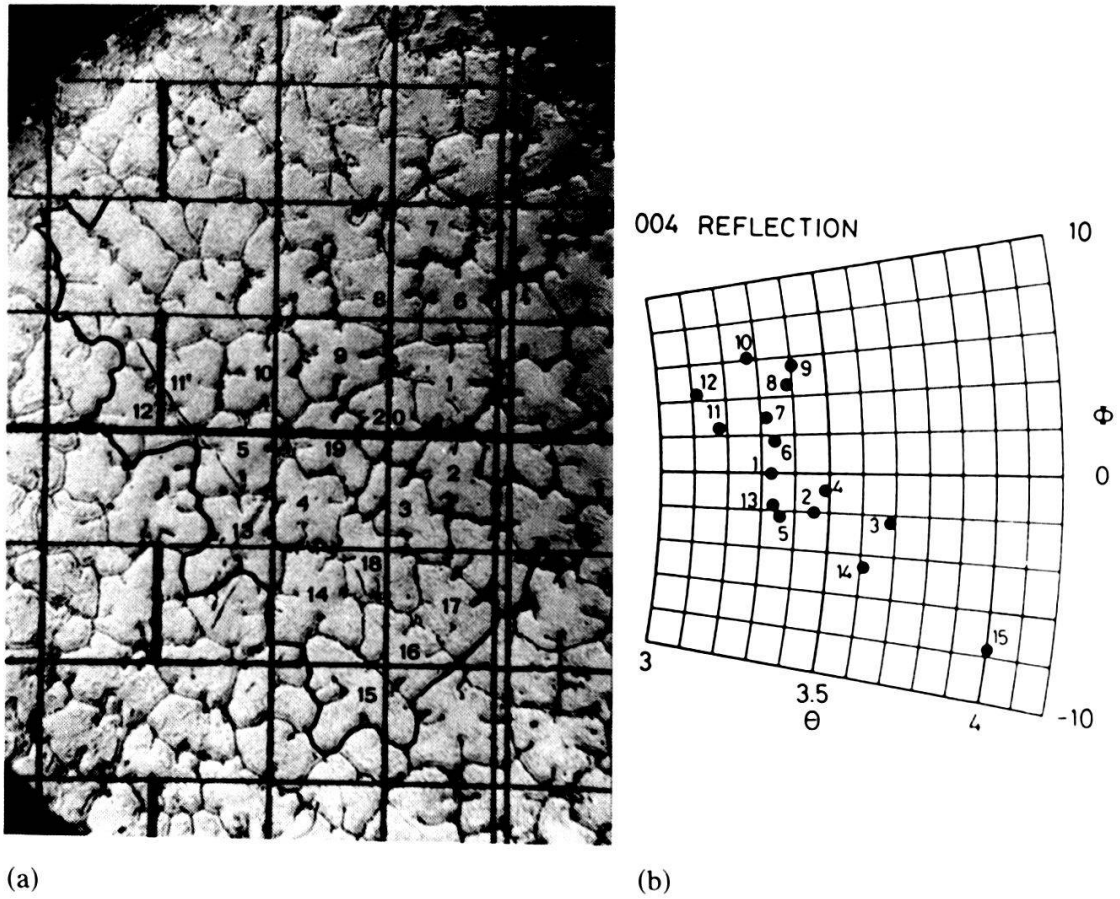


Figure 6
a) Transverse micrograph of a directionally solidified tricrystalline Ni–Cr–C alloy. b) Orientation distribution of dendrites #1–15 shown in Fig. 6a.

of the stereographic projection. Dendrite 15 which is surrounded in three directions by two other grains has an orientation quite different from all other dendrites. The average orientation of the numbered dendrites without those adjacent to the grain boundary, lies at $\bar{\theta} = 3.37°$ and $\bar{\phi} = 1.68°$ from the center of the stereographic projection while the solid angle defined by the standard deviation from the mean orientation, is $\Omega = 5.25 \cdot 10^{-5}$ steradian.

As a result from these diffractometric measurements it is concluded that dendritic single crystals are less perfect than those grown from pure metals with a planar solid–liquid interface. The crystallographic misorientations between adjacent dendrites may attain several tenths of a degree whereas the internal mosaic structures of individual dendrites are clearly better, typical values being smaller than one tenth of a degree [7]. Dendritic single crystals therefore contain a subgrain structure with a subgrain diameter in the order of the dendrite spacings.

## 3. Mechanical strength

The influence of microstructural inhomogeneities on tensile deformation has been determined in a recent investigation concerning the relationships between cast structures and mechanical properties. Ni–Cr–C alloys have been used as

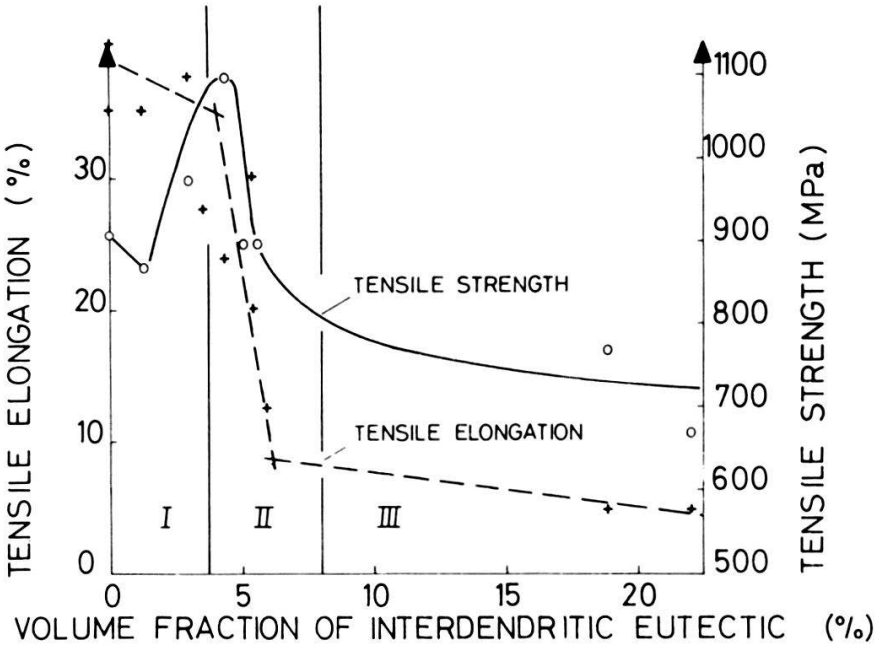


Figure 7
Tensile elongation and tensile strength of oriented Ni–Cr–C alloys vs. volume fraction of interdendritic eutectic.

model materials consisting of a ductile (Ni, Cr) solid solution matrix and brittle interdendritic $M_7C_3$ carbides.[5]) If tensile elongation and ultimate tensile strength are measured parallel to the dendrite growth axis as a function of the volume fraction of interdendritic eutectic, three composition ranges with different behaviours are observed (Fig. 7). In range I, there is only a minor influence of interdendritic carbides on ductility while the tensile strength increases with increasing volume fraction. Range II exhibiting more interdendritic precipitates is characterized by a drop of tensile strength and tensile elongation, both depending very much on solidification conditions as shown in Fig. 8. It should be noticed that the ductility passes through a maximum at medium size microstructures. Alloys with compositions belonging to range III exhibit a contiguous shell of brittle interdendritic eutectic. Tensile properties do not vary much in this range because, once a microcrack has been formed, it can easily propagate through the large brittle eutectic areas, thereby destroying the specimen.

Microcrack formation in these alloys can be predicted if the dendritic microstructure is considered to be a composite with a ductile dendritic solid solution and brittle interdendritic eutectic as the constituent phases [8]. In such a model which is shown in Fig. 9, the dendrite trunks represent ductile fibers embedded in a semi-brittle matrix comprising the dendrite arms and all interdendritic precipitates. Characterization of the effects of interdendritic precipitates on plastic deformation needs subdivision of the matrix into two kinds of elements. The first which is called $M_1$ in Fig. 9a, entirely consists of interdendritic eutectic separating the dendrite arms from each other. Their spacing is $\lambda_2$. The second

---

[5]) These alloys do not undergo allotropic transformations. Therefore, X-ray and electron diffraction techniques can be advantageously applied to their characterization in the as-solidified and the plastically deformed state.

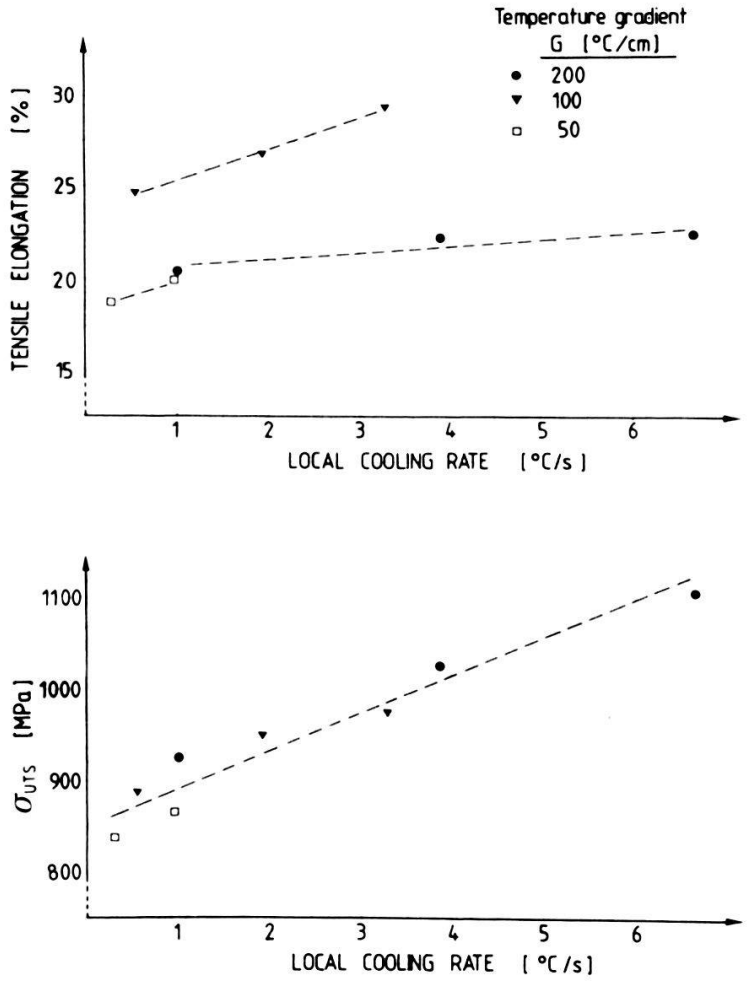


Figure 8
Tensile strength and tensile elongation of Ni-19% Cr-0.46% C alloys as a function of the cooling rate.

kind called $M_2$, contains the ductile dendrite arms and, additionally, the brittle eutectic precipitated between neighbouring dendrites. In order to rupture the brittle areas of thickness $t$ in element $M_2$, the composite must be deformed by:

$$\varepsilon_{M_2} = \varepsilon_R^e\left(1-\frac{b}{a}+\frac{t}{m}\right)+\frac{\sigma_{el}^s}{\theta^e}\left(1-\frac{t}{m}\right) \tag{7}$$

$\theta^e$ represents the work hardening coefficient and $\varepsilon_R^e$ the tensile elongation of the interdendritic eutectic. $\sigma_{el}^s$ is the solid solution yield stress. $\sigma_{el}^s$, $\theta^e$ and $\varepsilon_R^e$ characterize the properties of the constituent phases and can be measured separately. $b/a$ is the thickness ratio between $M_1$ and $M_2$. In correspondance with microstructural observations, it was assumed in equation (7) that $b/a \ll 1$. $b$ and $a$ are related to the dendrite arm spacing by $a+b=\lambda_2$.

Using the same nomenclature as in equation (7), rupture of the brittle elements $M_1$ should occur at a composite elongation of

$$\varepsilon_{M_1} = \varepsilon_R^e\left[1+\frac{m}{t}\left(1-\frac{b}{a}\right)\right]-\frac{\sigma_{el}^s}{\theta^e}\left(\frac{m}{t}-1\right)\left(1-\frac{b}{a}\right) \tag{8}$$

The ratios $b/a$ and $m/t$ which must be known in order to solve equations (7) and

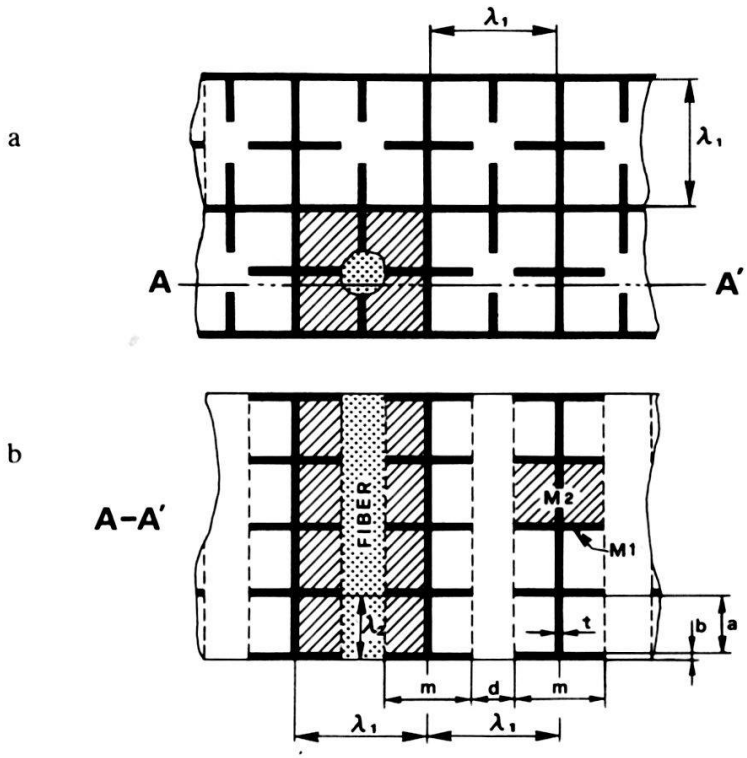


Figure 9
'Composite' – model of oriented dendritic microstructures. a) View transverse to the dendrite orientation; b) view parallel to the dendrites. The dendrite trunks represent ductile fibers embedded within a semi-brittle matrix. The interdendritic brittle eutectic is depicted by black bars while the remainder of the 'material' represents the dendrites itself which, in reality, consist of a ductile metallic solid solution.

(8) can be determined by quantitative metallography. Within the composition range II of Fig. 7, it is possible to relate the ratio $m/t$ to the dendritic microstructure by the following approximative formula:

$$\frac{m}{t} \simeq \frac{1}{f^e}\left[2-\left(\frac{d}{2\lambda_1}\right)^2\left(1+\frac{\pi}{2}\right)\right] \tag{4}$$

with $f^e$ being the eutectic volume fraction and $d$ the dendrite trunk diameter.

Equations (7) and (8) agree well with microscopic observations. Rupture of the brittle phase between neighbouring dendrites ($M_2$) already occurs after 1 to 2 percent deformation whereas the eutectic arms ($M_1$) oriented perpendicularly to the tensile axis typically break after 5 to 20 percent plastic deformation, depending on the geometry of the brittle phase distribution. Rupture of the eutectic arms leads to specimen failure if the dendrite trunks (fibers) are too thin to carry the entire load on the specimen. Both $\varepsilon_{M_1}$ and $\varepsilon_{M_2}$ depend on alloy composition and solidification conditions: early fracture initiation in elements $M_2$ is held back by a high eutectic volume fraction and by thick dendrite trunks whereas rupture of the more critical eutectic arms (elements $M_1$) is accelerated under the same conditions. In the latter case, the dendrite trunk diameter should be small if the eutectic volume fraction is high. Once the eutectic arms $M_1$ are broken, however, the unbroken dendrite trunks should be as thick as possible in order to avoid specimen failure.

The smallest repetitive element of the composite model discussed so far, has

the dimensions $\lambda_1^2 \cdot \lambda_2$ (Fig. 9). The stacking sequence of these elements does not enter into equations (7) and (8). All elements are assumed to deform independently from each other and to behave in exactly the same way. This assumption does not correspond to reality because slip lines at the specimen surface frequently extend over several elements. Furthermore, the slip line distribution follows the distribution of the interdendritic eutectic. It is therefore necessary to account for the stacking sequence of the basic elements of volume $\lambda_1^2 \cdot \lambda_2$: It can be seen from Fig. 1 that the dendrites are not randomly distributed within the single crystal. Along one direction, the dendrite arms are facing each other while in the perpendicular direction they are intercalated. Consequently, trunks are aligned in rows and successive rows are shifted by half a dendrite spacing.

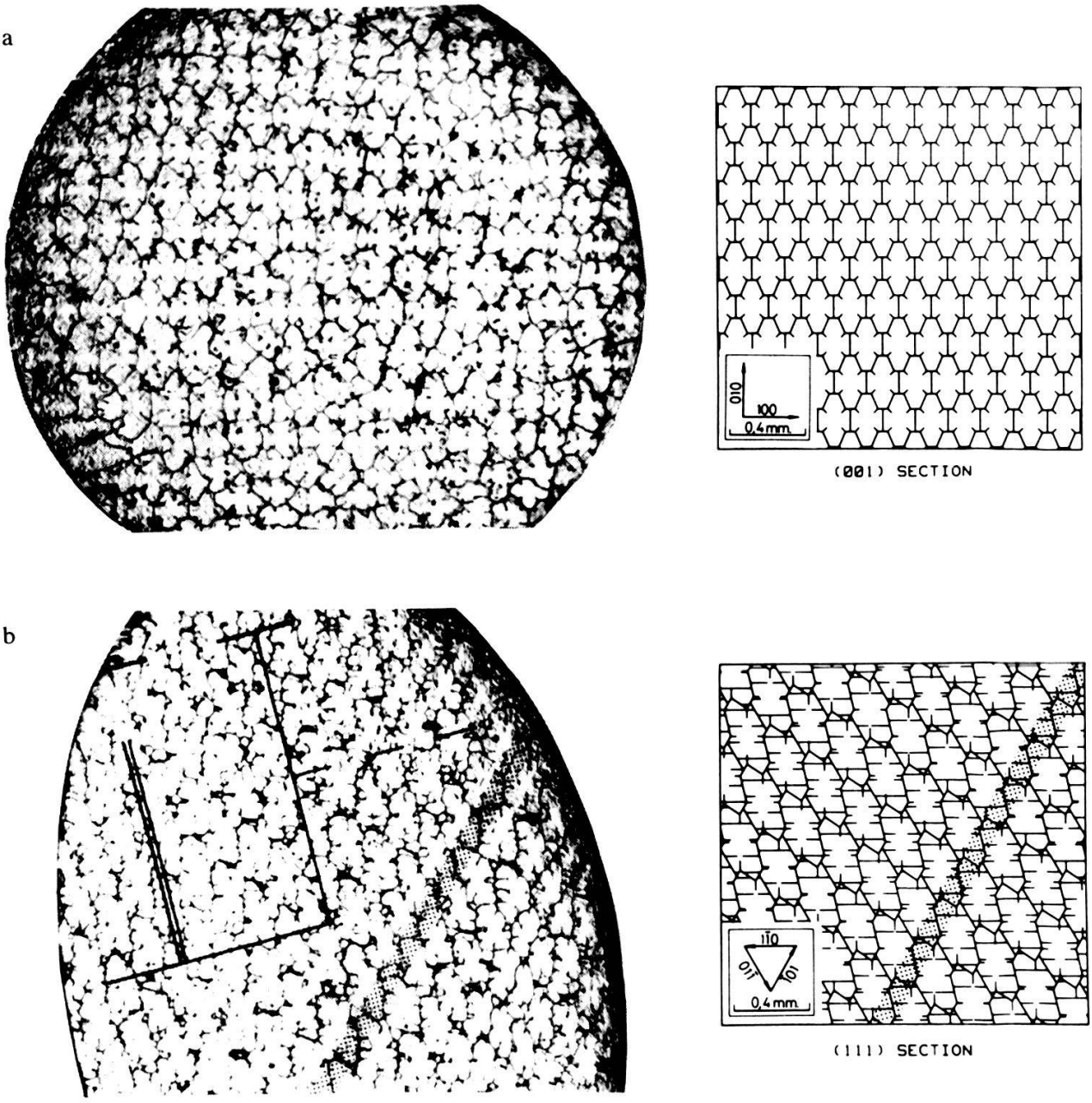


Figure 10
Comparison between real and computed sections of dendritic single crystals. Upper row (a): (001) crystallographic sections. Lower row (b): (111) crystallographic sections.

Such an arrangement can be described using the concept of a 'dendritic lattice' [9] in which the dendritic microstructure is simulated by a repetition of identical blocks, each having the volume $\lambda_1^2 \cdot \lambda_2$. The basis vectors of this lattice which is base-centered orthorhombic are parallel to the cubic axes of the crystallographic structure: their lengths are directly related to the dendrite motif since the space must be filled up without holes or overlaps. Figure 10 shows real and simulated (001) and (111) sections of such an ideal dendritic lattice. The (*hkl*) indices in Fig. 10 refer to the underlying crystallographic lattice (fcc). In these sections the interdendritic eutectic regions are visualized by dark segmented lines. [101] channels quite free of eutectic are clearly visible in the sections of type (111) (Fig. 10b). It can be demonstrated by X-ray topography and by X-ray microbeam diffraction [10] that the pattern of interdendritic precipitates represented by the dendrite lattice very strongly influences plastic deformation: in Fig. 11, representing the same primary (111) slip plane of a dendritic single-crystal as shown in Fig. 10, plastic deformation is localized on the already mentioned white [101] channels which are almost free from precipitates. Thus, the pattern of plastic deformation strictly follows the symmetry of the dendrite lattice which itself depends on the crystallographic anisotropy and the direction of heat flow in solidification.

The yield point of dendritic two-phase single crystals is determined by the solid solution matrix. Very high work hardening rates up to a tenth of Young's modulus during the first three percent of plastic deformation, result from the inhomogeneity of plastic deformation shown in Fig. 11. Analysis of operating slip systems indicates that the primary slip system is the system with the highest

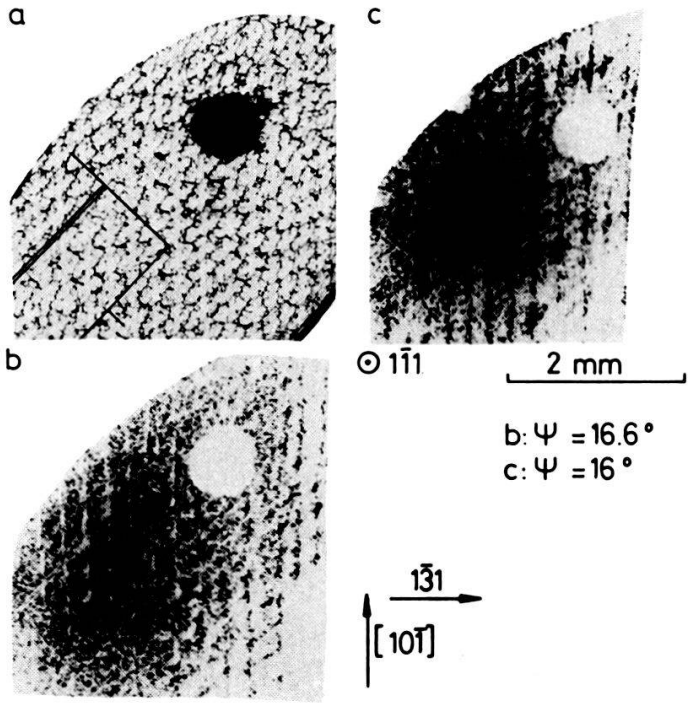


Figure 11
(111) crystallographic section of a dendritic Ni–Cr–C single crystal deformed by 2.5 percent. a) micrograph; b) and c) X-ray topograph showing a pattern of line contrasts coinciding with the carbide free channels of Fig. 11a. The dark lines in c) represent regions misoriented with respect to the remainder of the crystal. The misorientation is a result of localized plastic deformation. Contrast inversion as shown in Fig. 11c was obtained by a small rotation of the crystal with respect to the X-ray microbeam.

Schmid factor like in monophase single crystals. Since the interdendritic eutectic acts like microgrips which do not follow the shear deformation, secondary slip systems are activated for compensation of the back stresses exerted by the precipitates. X-ray microbeam diffraction has revealed the formation of a mosaic structure within individual dendrites during plastic deformation. It is concluded from these investigations, that modelling of dendritic two-phase microstructures as composite materials is appropriate to account for the effects of interdendritic precipitates on mechanical properties. In particular, microcrack formation which is a precursor to specimen failure, can be explained by this kind of a model describing the three-dimensional distribution of interdendritic precipitates in a rather concise way.

## 4. Conclusions

It has been shown in this paper how the microstructural dimensions of dendritic single crystals and the brittle phase distribution can be related to the kinetics of dendrite growth. A sequence of causal relationships extending from alloy composition, over liquid–solid phase transformation to mechanical properties has been established for the first time.

Microsegregations resulting from solidification have been known for long for their detrimental effects on fracture toughness. By the present investigation it was demonstrated that knowledge of the distribution of interdendritic eutectic is necessary in order to understand the plastic deformation behaviour of dendritic alloys. In tensile testing parallel to the dendrites, microcracking first appears in eutectis areas separating neighbouring dendrites (marked by letter $t$ in Fig. 9). These microcracks are not critical for the specimen strength, at least in the case of a ductile matrix which allows stress concentrations at the tips of microcracks to be relaxed by plastic deformation. Microcracking of eutectic areas extending perpendicularly to the tensile axis (elements $M_1$ in Fig. 9) is much more critical because, once these regions are broken, the effective load-bearing cross section of the specimen is considerably reduced. There is a twofold contribution of the dendrite trunks to plastic deformation. The bigger the trunk diameter the smaller the tensile elongation leading to the latter kind of microcracks. But after microcracking, big trunk diameters will increase the residual tensile elongation until rupture of the specimen.

Microcracking is preceded by plastic deformation. The localization of plastic deformation at areas free from carbides results in the formation of strain and stress gradients. It is not surprising that the 'degree' of localization is again determined by the distribution of interdendritic eutectic along the dendrite boundaries which, in some way, is characterized by the ratios of trunk diameter to primary dendrite spacing and trunk diameter to dendrite arm spacing. Strain and stress gradients give rise to microcracking of the interdendritic carbides. Specimen failure occurs by microcrack coalescence or by microcrack propagation. Crack propagation is facilitated by a continuous shell of interdendritic eutectic with major components of the shell extending perpendicularly to the main stress axis. Formation of a contiguous shell is essentially a question of alloy composition. Microcrack coalescence which becomes important at low volume fractions of interdendritic eutectic is a ductile fracture problem depending on the brittle phase

distribution and on the ratio of dendrite trunk diameter to dendrite arm spacing. Thus, plastic deformation and microcrack formation depend to a considerable extent on the distribution of interdendritic eutectic which is controlled by alloy composition and solidification conditions. This investigation confirms the empirically well known tendency that large dendrite arm spacings and large volume fractions of interdendritic brittle phases reduce toughness. Over that, modelling of the mechanical behaviour of dendritic alloys allows to determine critical microstructural parameters and to relate these to solidification.

The microstructural parameters like dendrite spacings and trunk diameter, entering into the description of the deformation behaviour measure the distribution of interdendritic eutectic in dendritic structures. Since the understanding of the interdependence of these parameters with alloy composition and heat flux conditions has been very much improved in recent years (for a review see [11]), control of mechanical properties via solidification control seems to become a more and more realistic goal in the near future. Single crystalline turbine blades only represent a first step in this development. Much wider application of the principles outlined in this paper is seen in advanced casting of Al–Si alloys for example, which find increasing use as structural parts in the automobile and aircraft industry [12].

## REFERENCES

[1] F. L. VERSNYDER and M. E. SHANK, Mat. Sci. Eng., *6* (1970) 213.
[2] E. SCHMID and W. BOAS, *Kristallplastizität*, Springer (Berlin 1935).
[3] J. S. LANGER, Rev. Mod. Phys., *52* (1980) 1.
[4] W. KURZ and D. J. FISHER, *Fundamentals of Solidification*, Trans. Tech., 1984.
[5] U. FEURER and R. WUNDERLIN, Fachbericht DGM, 1977.
[6] P. N. QUESTED and M. MCLEAN, Mat. Sci. Eng., *65* (1984) 171.
[7] M. RAPPAZ, M. KASPAR and E. BLANK, "Characterization of Microstructures by X-Ray Microdiffraction and Topography" in Proc. 5th Riso Int. Symposium on Metallurgy and Materials Science, Sept. 1984, p. 443.
[8] E. BLANK and M. RAPPAZ, "Plastic Deformation of Oriented Dendritic Alloys Containing Brittle Interdendritic Precipitates" in Colloques Internationaux du CNRS No. 319 "Comportement plastique des solides anisotropes", p. 257.
[9] M. RAPPAZ and E. BLANK, "The Concept of a Dendritic Lattice and its Use in Modelling of Oriented Dendritic Microstructures"; submitted for publication to J. Crystal Growth.
[10] M. RAPPAZ and E. BLANK, "Deformation Mechanisms of Dendritic Two-Phase Alloys studied by Means of X-ray Topography and X-ray Diffraction Techniques". Proc. 3rd Riso Int. Symp. on Metallurgy and Materials Science, 1982, p. 285.
[11] "30 Years after Constitutional Supercooling": Special Issue on Solidification, Mat. Sci. Eng., *65* (1984).
[12] D. MIETRACH and J. WEILKE, Aluminium, *58* (1982) 157.